An Acad Bras Cienc (2024) 96(Suppl. 2): e20240243 DOI 10.1590/0001-3765202420240243
Anais da Academia Brasileira de Ciências | *Annals of the Brazilian Academy of Sciences*
Printed ISSN 0001-3765 I Online ISSN 1678-2690
www.scielo.br/aabc | www.fb.com/aabcjournal

GEOSCIENCES

Glaciochemistry and environmental interpretation of a snow core from West Antarctica

REGINA S. FERREIRA, JEFFERSON C. SIMÕES, ISAÍAS U. THOEN & RONALDO T. BERNARDO

Abstract: This study investigated the chemical content of a shallow snow core (4.95 m) named TT 6, collected during a Brazilian traverse of the West Antarctic Ice Sheet in the 2014/2015 Austral summer. Stable isotope ratios (δD and $\delta^{18}O$) and ionic content, determined at the Centro Polar e Climático of the Federal University of Rio Grande do Sul (CPC/UFRGS), were used to date the core and reconstruct the climatic conditions at the site. The core represents approximately 11 years ± 6 months of precipitation, i.e., a mean net snow accumulation rate of 0.19 ± 0.02 m a^{-1} in water equivalent. Using the non-sea-salt sulfate values, we identified the 2011 Puyhue-Cordón (Chile) volcanic eruption signal, providing a reference horizon for dating. Anions represent 53.73% of the ionic content. We identified that 96.86% of calcium and 84.50% of sulfate are non-sea origin, while the acidic contribution is 25.62% H^+. We observed high peaks in marine aerosols containing Na^+, Cl^-, and Mg^{2+} during winter, and results from the ERA5 global model (NOAA) indicated that El Niño events could influence Antarctic temperatures, facilitating the transport of marine aerosols to the continent.

Key words: ice core, West Antarctica, major ions, marine aerosol, Glaciochemistry.

INTRODUCTION

The Antarctic ice sheet has unique features that allow for preserving past climate records and reconstructing high-resolution historical series. Using this data, we can recreate past climate patterns to understand recent changes and forecast anomalous behavior impacts. Despite being a climate-sensitive region, the West Antarctic Ice Sheet (WAIS) has a lower data coverage of information than other Antarctic regions.

The WAIS bedrock elevation is lower than the rest of the continent, having its crustal portion below sea level. This factor exposes the glacier front to direct contact with the seawater, increasing the risk of collapse with rising ocean temperatures (Nicolas & Bromwich 2011). In addition, record warming events and extensive melting (Nicolas et al. 2017) have been detected in the region. They are associated with the influence of large-scale climate modes, such as the El Niño–Southern Oscillation (ENSO) phenomenon.

Since the late 1950s, snow and ice cores have been used as high-resolution proxies (indirect evidence) of past environmental changes. By determining the chemical characteristics of their content, it is possible to estimate the environmental conditions at the time of the ice crystal condensation, precipitation, and deposition, such as temperature, local accumulation of snow, aerosol deposition, and greenhouse gas concentrations.

Among the various glaciochemical analytical techniques, we highlight the investigation of the variability of stable water isotope content. The seasonal precipitation pattern of $\delta^{18}O$ or δD helps date snow and ice cores. According to the Rayleigh fractionation model, precipitation in an equilibrium state changes mainly according to the temperature variation (Jouzel 2013), which can be associated with changes in altitude, latitude, and seasonality of the site of interest and the moisture source area.

Using ion chromatography (IC) allows the identification of chemical species in snow and ice samples. This approach enables the identification of potential source areas, reconstruction of atmospheric transport patterns, and investigation of climatic characteristics of the study region. Understanding the behavior and seasonality of a chemical species helps to determine the characteristics of air masses bringing the precipitation; for example, Na^{+}, in general, is more abundantly in winter, and this is attributed to the formation of frost flowers, which serve as an effective source of sodium for the atmosphere (Wolff et al. 2003).

This study determined the content of stable isotopes and the main ions in a snow and firn core (the intermediate state of the snow-to-ice metamorphism) to reconstruct the site's climatic conditions and seek environmental interpretations of the region. This core, called TT-6, was collected in WAIS during the first Brazilian Antarctic traverse in the Austral summer of 2014/2015.

MATERIALS AND METHODS

The TT-6 site (study area)

During the 2014/2015 traverse, the team of CPC/UFRGS recovered 8 shallow snow and firn cores, ranging from 5 to 20 m deep. TT-6 was collected on January 12, 2015 at 80°24'54.9" S, 94°41'03.2" W (Figure 1), at a 2,123 ± 10 m altitude and about 700 km from the Amundsen Sea coast. This site is within the Pine Island Glacier (PIG) drainage basin, considered one of the most dynamic and unstable Antarctic ice masses (Jakobsson et al. 2012, Lindow et al. 2014).

Initial processing of samples

At the Climate Change Institute in Maine (CCI), Orono, Maine, USA, the samples underwent decontamination in a cold room (-20°C), where ceramic knives scraped the surface and ends of each core section. The TT-6 was melted using a continuous melting system at the CCI (Osterberg et al. 2006). The snow or ice core is held vertically by an acrylic support inside a freezer; the core base sits on a heated nickel plate (99.99% Ni) with a ring that separates the inner and outer parts; the melted content is then directed into collection vials. The outer content is used for isotopic analyses, while the innermost (and consequently with a lower risk of contamination) is used for ion chromatography (IC). This process was applied to all 5 sections of the TT-6, each approximately 1 meter long. After melting each section, a cleaning protocol was used, including flushing the entire drainage system with Citranox detergent solution and rinsing it with purified water for 30 minutes (Thoen 2017). To identify potential residues of Citranox, "blank" samples were collected and underwent the same chemical analyses explained below.

Isotope analysis

Isotope analyses were carried out in the Stable Isotopes laboratory at the CPC/UFRGS, using a Picarro® system consisting of a Ring-down Cavity Spectrometer with three Isotopic H_2O L2310-i mirrors and an Isotopic H_2O V1102-i vaporization module, which is powered by hydrogen gas injection.

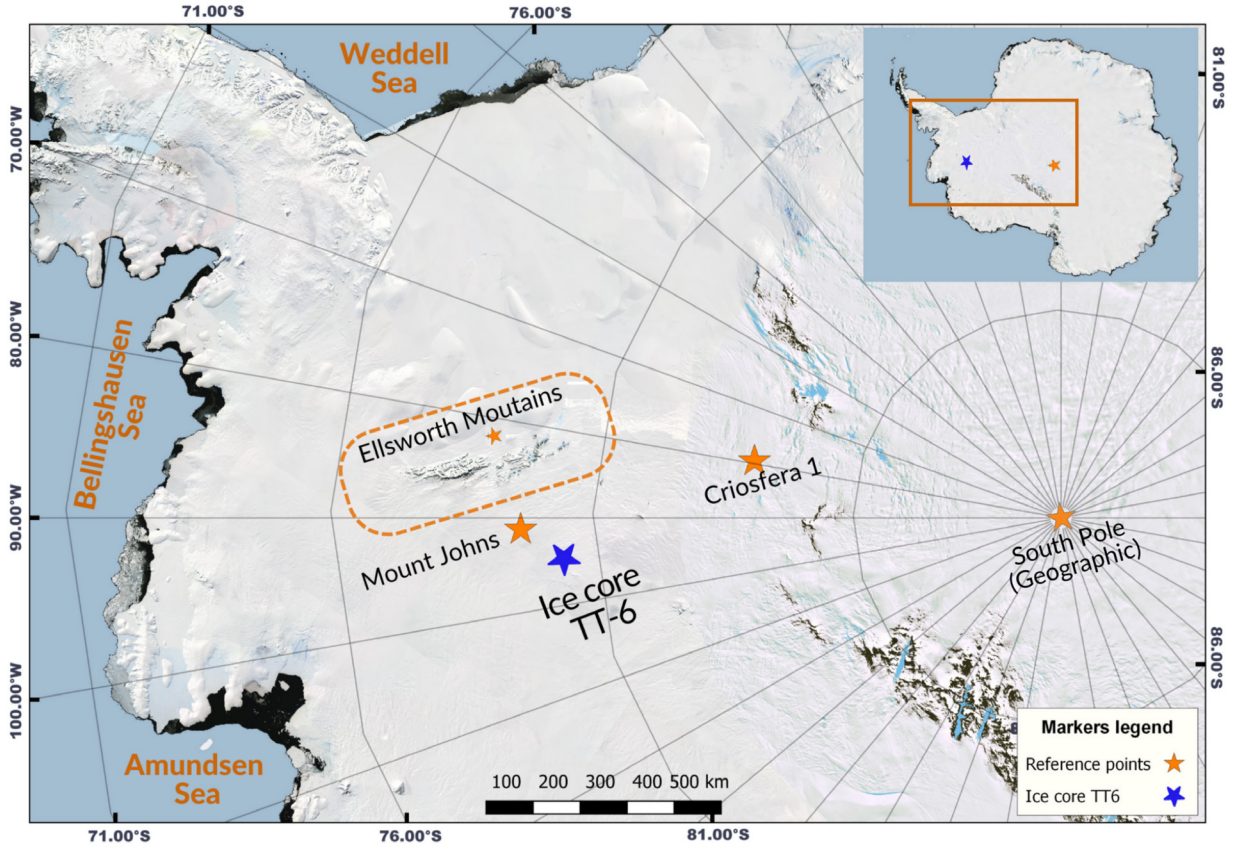

Figure 1. Location map showing the TT-6 core site (80°24'54.9" S, 94°41'03.2" W) marked by a blue star, along with other reference points cited in this study, indicated by orange stars: Mount Johns, the Ellsworth Mountains, and Criosfera 1. The Weddell, Bellingshausen, and Amundsen seas are highlighted in orange to provide geographical context. Source: Quantarctica database and authors.

The snow and firn samples were thawed, 25 units at a time, and sub-sampled by pipetting into 2 mL vials in the automatic sampler, interspersed with 12 vials of the laboratory's in-house standard solutions. Calibration is performed with two rounds of analysis using only internal standards, which are calibrated using certified standards (SLAP – Standard Light Antarctic Precipitation and GISP – Greenland Ice Sheet Precipitation); these results are adjusted in Excel with the calibration curves of the certified standards and, finally, each internal standard has its average calculated with the values of the two rounds. The standards used were the low-$\delta^{18}O$ SPOLE II (content sampled at the Geographic South Pole), high-$\delta^{18}O$ MJ2 (content collected at Mount Johns ice core site, WAIS), and a reference standard TT-01 (content collected in the region of the Brazilian Criosfera 1 scientific module; 84°S, 79.5°W, WAIS). Each sample was divided by the equipment into 8 sub-samples so the equipment could acclimatize, reducing the memory effect (remnants of the previous sample). The raw data is extracted from the system in Excel spreadsheets, and only the results of the last three analyses are considered to create calibration curves for the results.

Ion chromatography

The IC analyses were carried out in the clean room of the Isotopic Geology Laboratory (LGI) at the CPC/UFRGS. The room has a ventilation

system and a laminar flow hood with a High Efficiency Particulate Air (HEPA) filter to reduce the risk of sample contamination.

Before analysis, the equipment is given a specific configuration (Table I) and calibrated by running samples of known values, with which the integration calculations for each analyte are adjusted. The solutions are prepared for anions and cations, the so-called calibration points for this procedure. They are produced using the standard solutions from Quimlab SpecSol, combining the analytes of interest in the intermediate solutions AIS and CIS, which are then diluted to 5 different concentrations each, A1, A2, A3, A4 and A5 and C1, C2, C3, C4 and C5, which have increasing concentration values.

After a rigorous process of material cleaning (as described by Thoen 2017), the 157 samples were thawed and transferred to 5 mL vials. Once prepared, these were placed in the sampler and interspersed with vials with MilliQ® water and internal standards for control. The selected standards were A4, C4, and BM2. The analyses were conducted using two Thermo Scientific® chromatographs, one anion, and one cation system, which analyzed the injected content simultaneously. Each sample underwent a 27-minute analytical process, illustrated in Figure 2, displayed through the Chromeleon® software, generating real-time viewable chromatograms. Subsequently, the integration intervals of all analytes in each sample were confirmed, with manual adjustments made when necessary to ensure that the program includes even the lowest detected ion values in the calculation.

Climate Analysis

To better understand the atmospheric behavior during the snow core precipitation, we used the reanalysis product of the global ERA 5 model, developed by the ECMWF (European Centre for Medium-Range Weather Forecasts). The reanalysis methodology merges numerical modeling with observational data, rectifying potential model inaccuracies and generating results that are more congruent with actual conditions.

Due to the characteristics of the geometric ERA5 model grid, which is geometric and has a resolution of 0.25°, it is impossible to extract data directly from a point of interest. According to Hersbach et al. (2020), when requesting data from a specific location, the model performs bilinear interpolation of the available data to the area of the grid in which the requested location is located. Then, the data generated for the region around the TT6 site was worked on

Table I. System configuration used for ion chromatography.

Components	Anions (ECD-1)	Cations (EDC-2)	Brand
Model	ICS200	ICS2100	Thermo Scientific®
Analytical Column	AS-18 2 mm	CS-18 2 mm	Ion Pack®
Guard Column	AG-18	CG-19 4 µm	Ion Pack®
Temperature	35 ± 0.1°C	35 ± 0.1°C	-
Loop	200 µL	200 µL	-
Suppressor	AERS 500 2 mm	CDRS 600 2 mm	-
Detector	CD20	CD20	-
Eluent type	KOH	MSA	Elugen®

at coordinates -80.25° N, -80.50° S, -93.50° E and -95.50° W.

The chosen product was the ERA5 monthly averaged data on single levels from 1940 to the present, with a download of the monthly averages of the variables:

- Snow albedo (reflectivity measured on a scale from 0 to 1, without a specific unit) from January 2004 to January 2015,

- Temperature at 2 meters above the surface (provided in Fahrenheit) from January 2004 to January 2015, but considering only the months of January, April, July, and October, each representing a climatic season of the year.

The product ERA5 hourly data on single levels from 1940 to the present with the download of the variable, extracted for all days between January 2004 and January 2015:

- Snowfall (in meters of water equivalent),

- Components u (eastward) and v (northward) of the wind, at 800 hPa, due to the height of the ice sheet.

RESULTS

The raw dataset from the TT-6 snow core analysis, comprising ion chromatography and resonant cavity spectrometry (isotope analysis) results, is publicly accessible on Zenodo (Ferreira 2024). This open-access resource promotes transparency and facilitates future research and replication within the scientific community.

Dating and density

Measuring the solid snow core's length, diameter, and weight allowed us to calculate each section's density and convert it to the equivalent water depth as the volume of the sample in its liquid state. A stratigraphic profile was constructed before melting the core. In Figure 3, sharp changes in density are related to depth hoar or ice lenses.

The mean density of the core is 0.43 g cm^{-3} (ranging from 0.26 g cm^{-3} to 0.52 g cm^{3}), values that represent snow in the upper three meters, followed by firn to the base. Ice lenses are present throughout the length of the core, and

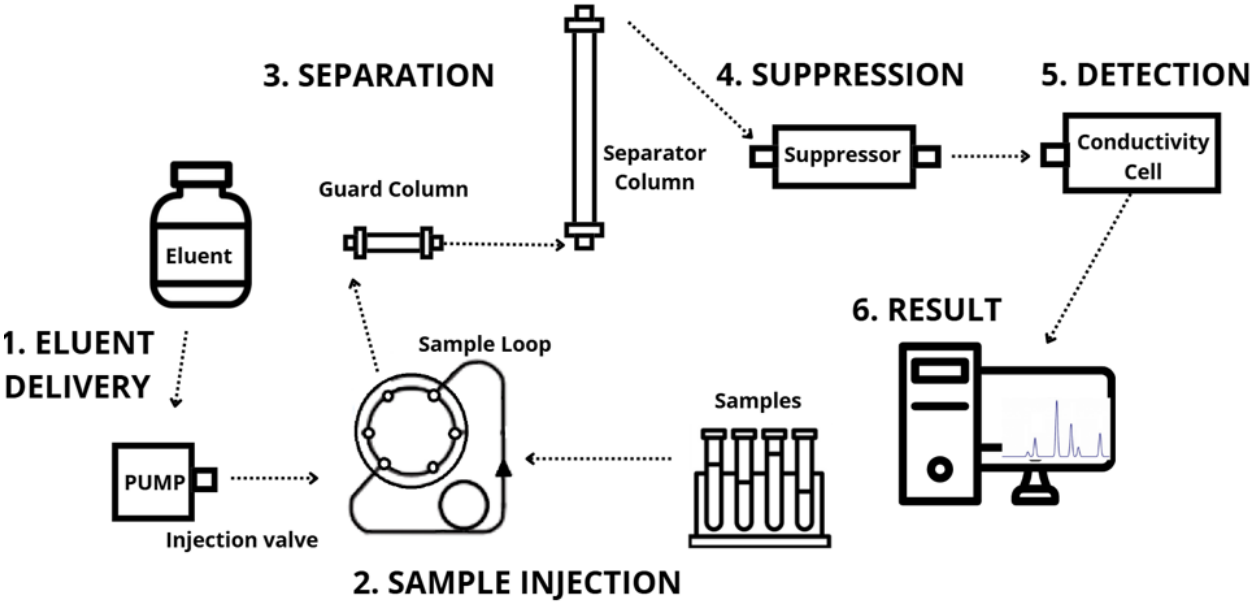

Figure 2. Flowchart of the ion chromatography analysis process, demonstrating the main steps: "1- Eluent Delivery", "2- Sample Injection", "3- Separation", "4- Suppression", "5- Detection", "6- Result", and listing which system components are related to each step. Source: authors.

layers of depth hoar were identified only in the first and fourth meters of depth.

Dating was performed using annual layer counting, an efficient technique for sites with a high accumulation rate (Schwanck 2016). For this technique, the non-sea-salt sulfate profile ($nssSO_4^{2-}$, from a crustal source, in this case, estimated to be of volcanic origin) was used, which allowed us to identify the peak attributed to the 2011 eruption of the Puyehue-Cordón Caulle volcano (this process is detailed in Section "Ions") and using the $\delta^{18}O$ time series compared to variations in the $nssSO_4^{2-}$ / Na^+ ratio. In this ionic ratio, the peaks were considered the apex of summer and marked the beginning of a year; these are indicated by vertical gray lines in Figure 4. In the individual graphs of $nssSO_4^{2-}$ and Na^+, due to the inverse behavior of these chemical species, the peaks (maximum value) of $nssSO_4^{2-}$ can be aligned with the valleys (minimum value) of Na^+.

These observations estimated that TT-6, with a depth of 4.95 m in solid state, is 2.1 m in equivalent water depth, representing 11 years, ± 6 months. This uncertainty was calculated using linear regression, applied to the correlation between depth and estimated years, thereby obtaining the error of the angular coefficient X. Therefore, we understand that the content of TT-6 corresponds to the period from 2004 to 2015 CE (Current Era).

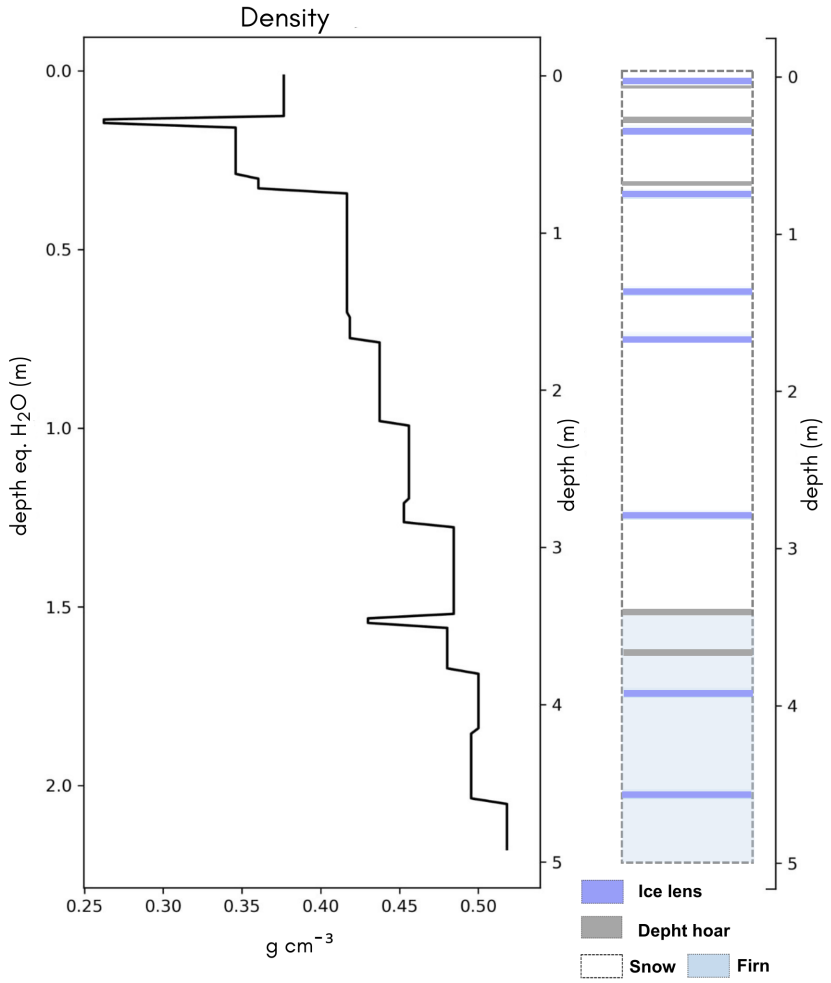

Figure 3. Density (left) and stratigraphic (right) profiles of the TT-6 snow core. The figure shows both the true depth and the water-equivalent depth. Gray bands represent depth hoar in the stratigraphic profile , while blue bands indicate ice lenses. Source: authors.

Isotopes

To interpret the variations in the stable isotopic composition of the samples, the straight-line equation (linear regression) of the δD and $\delta^{18}O$ relationship was calculated and compared to the Global Meteoric Water Line (GMWL) (Craig 1961), see Figure 5. This graph also shows the Antarctic Meteoric Line determined by Masson-Delmotte et al. (2008) and the TT-6 isotopic samples (represented by gray circles). The TT-6 samples are close to the meteoric lines. The coefficient of determination of the TT-6 line (R^2) at 0.99% indicates that the linear model is statistically representative. This relationship may also suggest that no significant refreezing or melting events in the material, from the collection area to the sampling, could significantly interfere with the results' quality.

The simple statistical results obtained for $\delta^{18}O$ and δD (Table II) are within the range of values found in this sector of Antarctica found by a study of surface samples along the entire 2014/2015 crossing (Marcher et al. 2022).

Ions

Simple statistical calculations were applied to the ion chromatography results, thus obtaining each analyte's range and mean concentrations (Table III). The last column indicates the number of samples in which each ion was detected in sufficient quantity to be integrated by the

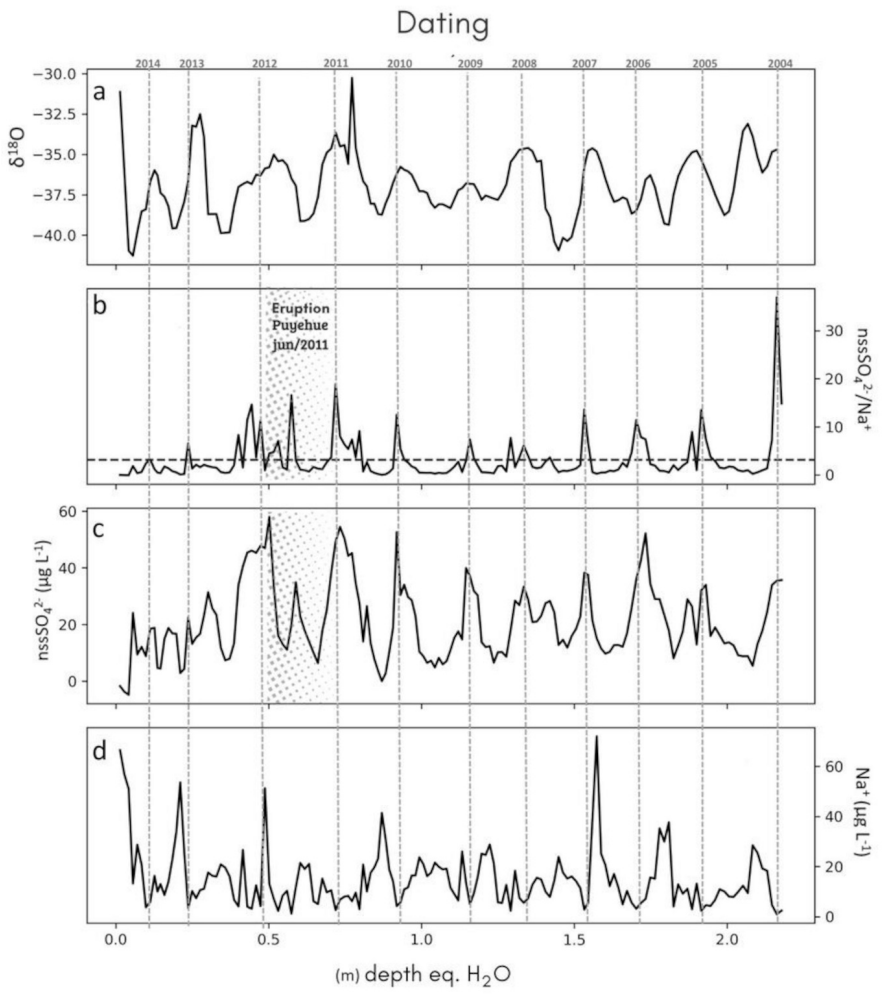

Figure 4. Profiles of $\delta^{18}O$ (a), $nssSO_4^{2-}/Na^+$ ratio (b), $nssSO_4^{2-}$ (c), and Na^+ (d) show seasonal variations. They were used to date the TT-6 core. The hatched area in Figures (b) and (c) identifies the signal of the 2011 Puyehue-Cordón Caulle volcano eruption in Chile. The dotted line in Figure (b) marks the mean $nssSO_4^{2-}/Na^+$ ratio. Source: authors.

software, generating a visual elevation in the chromatogram and a result in the output table.

The $nssSO_4^{2-}$ values were obtained using the equation 1 *nssS*

$4\ 2- = SO_4^{2-} - (0.251 \times Na^{+})$ (Dixon et al. 2004). This allowed us to determine the influence of volcanic-origin sulfate (i.e., non-marine) and identify reference horizons useful for dating. To correlate the $nssSO_4^{2-}$ peaks with volcanic events, we searched the Global Volcanism Program (GVP) database maintained by the Smithsonian Institution. which is part of the National Museum of Natural History in Washington D.C., USA. We considered confirmed eruptions with a Volcanic Explosive Index (VEI) greater than 4 between January 2004 and January 2015 (Table IV). The eruption referenced in the dating was the Puyehue-Cordón Caulle eruption, which took place in Chile on June 4, 2011. This eruption was classified as IEV 5, the highest level within the analyzed period, and exhibited rapid material dispersion toward Antarctica (Schipper et al. 2013). The identified $nssSO_4^{2-}$ peak falls between 2011 and 2012 and corresponds to a value three standard deviations above the mean.

Each ion mean concentration in the TT-6 core was transformed into a percentage to show the concentration of each analyte in the sample. Figure 6 shows that the anions have a more significant presence than the cations.

Table II. Sable isotopic values in the TT-6 snow core.

	Minimum	Maximum	Mean	Standard Deviation
$\delta^{18}O$	-41.27	-30.27	-36.96	1.90
δD	-323.99	-237.69	-290.46	15.72

Table III. Ionic concentrations in the TT-6 snow core.

Concentration of analytes (μg L^{-1})						
	Ions	Mean	Minimum	Maximum	Standard Deviation	Samples*
Anions	$CH_3SO_3^-$	5.98	0.39	41.21	22.13	135
	Cl^-	26.97	4.79	119.87	61.05	157
	NO_3^-	38.01	12.5	73.96	30.88	155
	SO_4^{2-}	26.37	3.79	71.20	34.31	157
	$nssSO_4^{2-}$	22.50	0.01	71.20	36.39	157
	$C_2O_4^{2-}$	1.45	0.41	11.37	6.05	144
Cations	Na^+	16.29	1.91	72.80	37.47	157
	NH_4^+	18.70	1.38	80.54	41.61	146
	K^+	3.38	1.31	25.59	13.46	66
	Mg^{2+}	1.71	0.56	7.32	3.62	154
	Ca^{2+}	11.94	4.00	142.54	77.80	153

***Due to the very low concentration of some ions, the chromatograph sometimes could not capture their amounts. Therefore, some analytes were not recorded in some samples.**

Table IV. Volcanic Explosion Index (VEI) above 4 from 2004 to 2015, as listed in the Global Volcanism Program (GVP) maintained by the Smithsonian Institution (https://volcano.si.edu/).

Volcano	Location	Eruption start date	VEI	Volcano type
Manam	New Guinea	October 24, 2004	4	Stratovolcano
Chaiten	Chile	May 2, 2008	4	Caldera
Kasatochi	USA	August 7, 2008	4	Stratovolcano
Sarychev Peak	Russia	June 11, 2009	4	Stratovolcano
Merapi	Indonesia	October 26, 2010	4	Stratovolcano
Puyehue-Cordon	**Chile**	**June 4, 2011**	**5**	**Stratovolcano**
Nabro	North Africa	June 13, 2011	4	Stratovolcano
Sinabung	Indonesia	September 15, 2013	4	Stratovolcano
Semeru	Indonesia	April 1, 2014	4	Stratovolcano
Manam	Papua Guinea	June 29, 2014	4	Stratovolcano

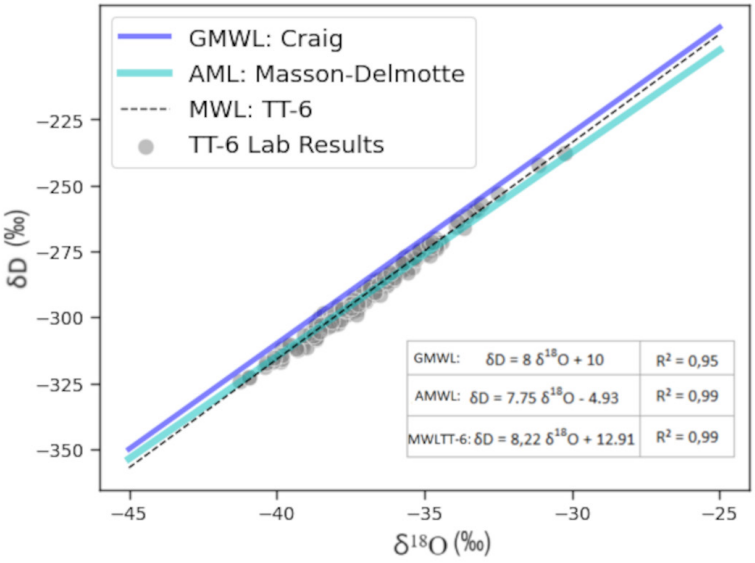

Figure 5. Linear relationship of $\delta^{18}O$ and δD in Antarctic samples (AMWL, blue line, Masson-Delmotte et al. 2008) and from this study (MWLTT-6, black dashed line), compared to the Global Meteoric Water Line (GMWL, purple line) from Craig (1961). The bottom-right inset shows the equations used to calculate each line. Source: authors.

Climatic Conditions with ERA5 reanalysis

The reanalysis data from the ERA5 model was processed using various software programs to generate figures that effectively illustrate the seasonal patterns of each variable. These patterns are displayed in tables and graphs and help observe the relationship between chemical and meteorological data.

Temperature

Table V presents two temperature extremes (minimum and maximum) for each season between 2004 and 2015. It reveals no clear pattern in the temperature extremes during this period. There were no consistent trends, such as an entirely colder or warmer year, as the minimum or maximum temperatures for each

season were not consistently recorded in the same year. Additionally, it is noteworthy that the year with the highest mean temperature does not necessarily align with the year with the hottest summer. This lack of consistency persists for the lowest temperatures as well.

Figure 7 illustrates the temperature patterns throughout each year in detail, highlighting October 2005 and 2006, particularly July 2011 (winter period), where temperatures were unusually close to -30°C, which can be considered warm compared to other years in the studied period.

Accumulation Rate

The accumulation rate is derived from the ratio between the length of the core (in this case, converted to equivalent meters of water) and the estimated number of years. A graph is plotted to depict the relationship between these two variables to extract a linear equation, where the angular coefficient value represents the mean accumulation rate. The standard error denotes the variance of this rate. TT-6 core has 2.18 m eq. of H_2O and approximately 11 ± 6 months, resulting in a snow accumulation rate of 0.19 ± 0.02 m yr^{1} as shown in Figure 8. This value is close to that of Schwanck (2016), who obtained a mean accumulation rate of 0.21 m yr^{-1} in H_2O equivalent for the Mount Johns site.

For comparison purposes, Figure 9 presents snowfall data from the ERA5 reanalysis, indicating an average accumulation of 0.12 m of water equivalent per year. This value

Table V. Temperature extremes (°C) between January 2004 and January 2015.

	Lowest Temperature		Highest temperature	
Annual mean	2004 →	-31.99	2005 →	-30.55
Sumer (January)	2009 →	-23.40	2007 →	-18.59
Autumn (April)	2013 →	-35.79	2014 →	-30.16
Winter (July)	2004 →	-42.45	2011 →	-29.33
Spring (October)	2007 →	-36.42	2006 →	-29.28

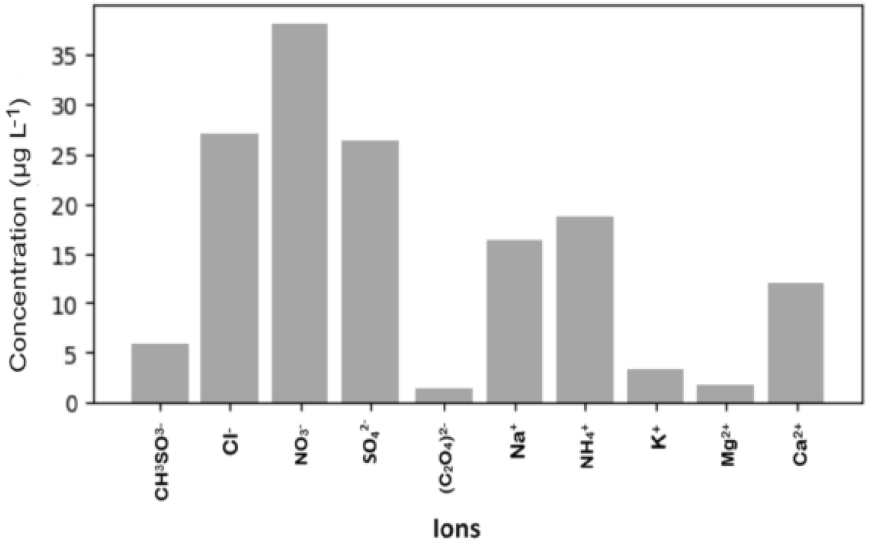

Figure 6. Graph of the mean analyte concentrations in the chemical composition of TT-6. Source: authors.

is underestimated as it solely considers the estimate of atmospheric precipitation. It does not account for potential accumulations of wind-driven snow (i.e., drifting snow) or vapor crystallization on the surface. Nonetheless, it can serve as an approximate reference for values.

The albedo recorded during the period of interest remained between 0.8 and 0.9, typical values associated with snow (generally >0.8 (Hersbach et al. 2023). This suggests that particles resulting from the 2011 eruption, which could have reached the TT-6 area in the form of tephra and interfered with surface reflectivity, did not impact the local albedo.

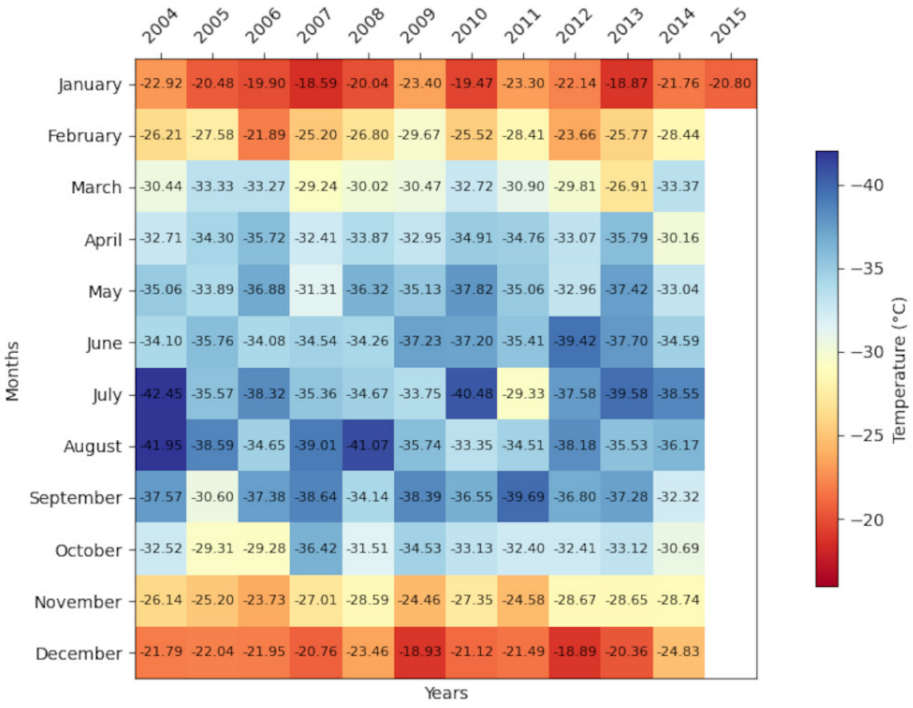

Figure 7. Heat map illustrating the variation in mean monthly temperatures from January 2004 to January 2015, with a gradient scale where more negative temperatures are represented by shades of blue, and less negative temperatures by shades of orange. Created using ERA5 reanalysis model data (temperature at 2 meters above the surface). Source: authors.

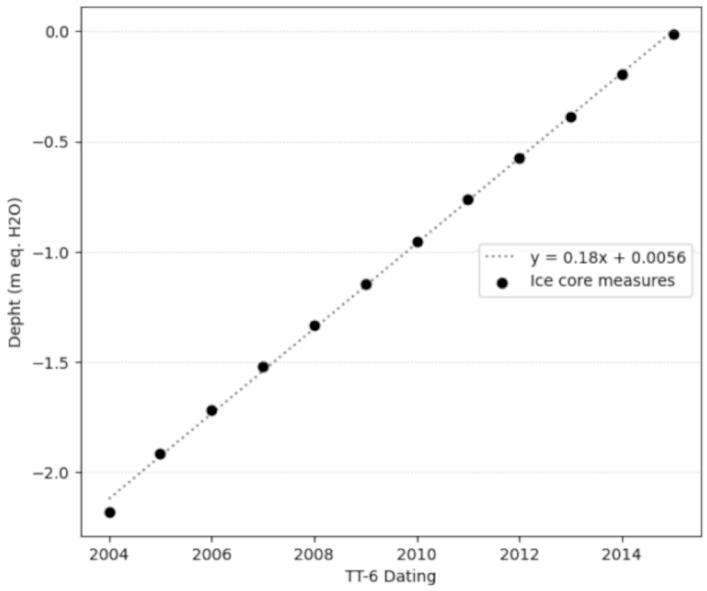

Figure 8. The relationship between depth (m eq. H_2O) and dating (years) for the TT-6 snow core shows the linear trend used to estimate the snow accumulation rate over time. The scatterplot represents ice core measurements (black dots), while the dashed line shows the linear equation y = 0.18 x + 0.0056 y=0.18x+0.0056, indicating a consistent accumulation rate from 2004 to 2015. Source: authors.

Wind

The u and v components of the wind allowed the calculation of direction and speed, indicating a predominance of winds from the south and southwest (Figure 10). Considering the entire period analyzed, the average value of 18 km h^{-1} and monthly maximums of 75 km h^{-1} recorded in November 2011 are equivalent to those observed in Patriot Hills (80°18'S; 81°22'W) by Turner & Pendlebury (2004).

DISCUSSION

Detailed ionic composition and ionic balance

The cation content equals 46.34% of the total ions, and the acidic contribution, which represents the capacity of these aerosols to release hydrogen ions and lower the pH of the environment, was obtained using equation 2 (adapted from Legrand & Mayewski 1997), with H^+ predominating at 25.62%.

Equation 2:

$$H^+ = \{[MS^-] + [Cl^-] + [NO^{3-}] + [SO_4^{2-}]\} - \{[Na^+] + [K^+] + [Mg^{2+}] + [Ca^{2+}]\}$$

Anions account for 53.76% of the ionic composition of TT-6. Light chain carboxylic acids ($HCOOH^-$, CH_3COO^-, and $C_2O_4^{2-}$) account for 13.68% of the total ions and are of photochemical origin when present in the atmosphere (Thoen 2017).

By summing the means of the major ions, we obtain 16 µEq L^{-1}. This value falls within the mean global snow composition limits, between 5 and 30 µEq L^{-1}, as established in the polar glaciochemistry review (Legrand & Mayewski 1997). Figure 11 depicts the entire distribution of analytes.

Correlation and source estimation of ions

To identify the relationship between ions, a correction matrix (Figure 12) was constructed using a statistical calculation of "Pearson's r" (correlation coefficient) between pairs of variables to estimate possible common source areas. With an index ranging from -1 to +1, the matrix determines the agreement between the values of two analytes. Positive values indicate simultaneous increases in variables, and negative values indicate an inverse relationship (Anzano et al. 2022).

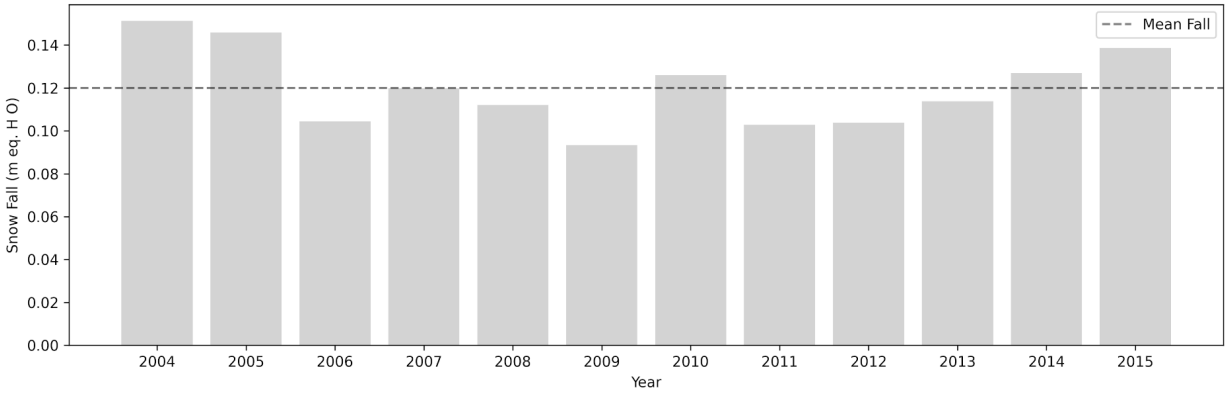

Figure 9. Annual accumulation rate at the TT-6 site, created from model ERA5 reanalysis data. The dashed line represents the overall mean annual accumulation rate for the study period (2004–2015). Source: authors.

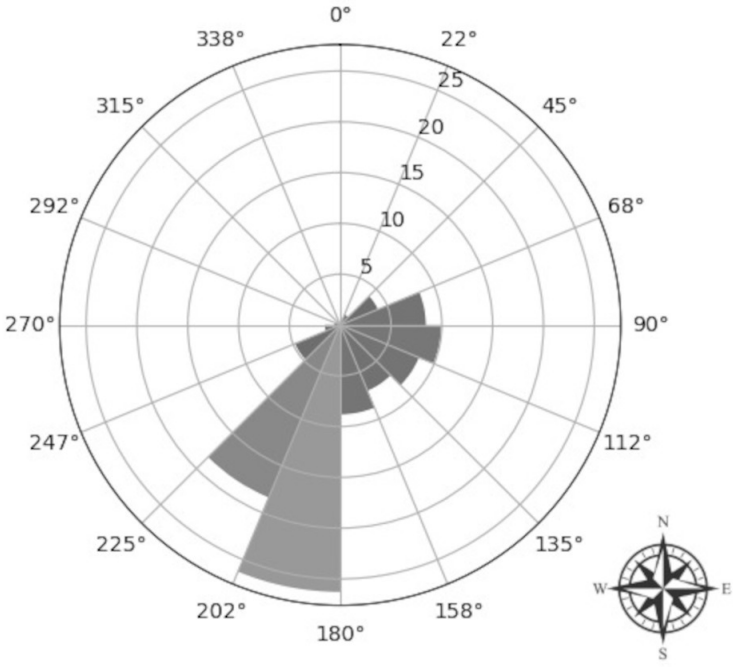

Figure 10. Wind rose showing the direction and speed of the u and v wind components at the TT-6 site from 2004 to 2015, based on ERA5 reanalysis data. A predominance of winds from the south-southwest quadrants is observed. Source: authors.

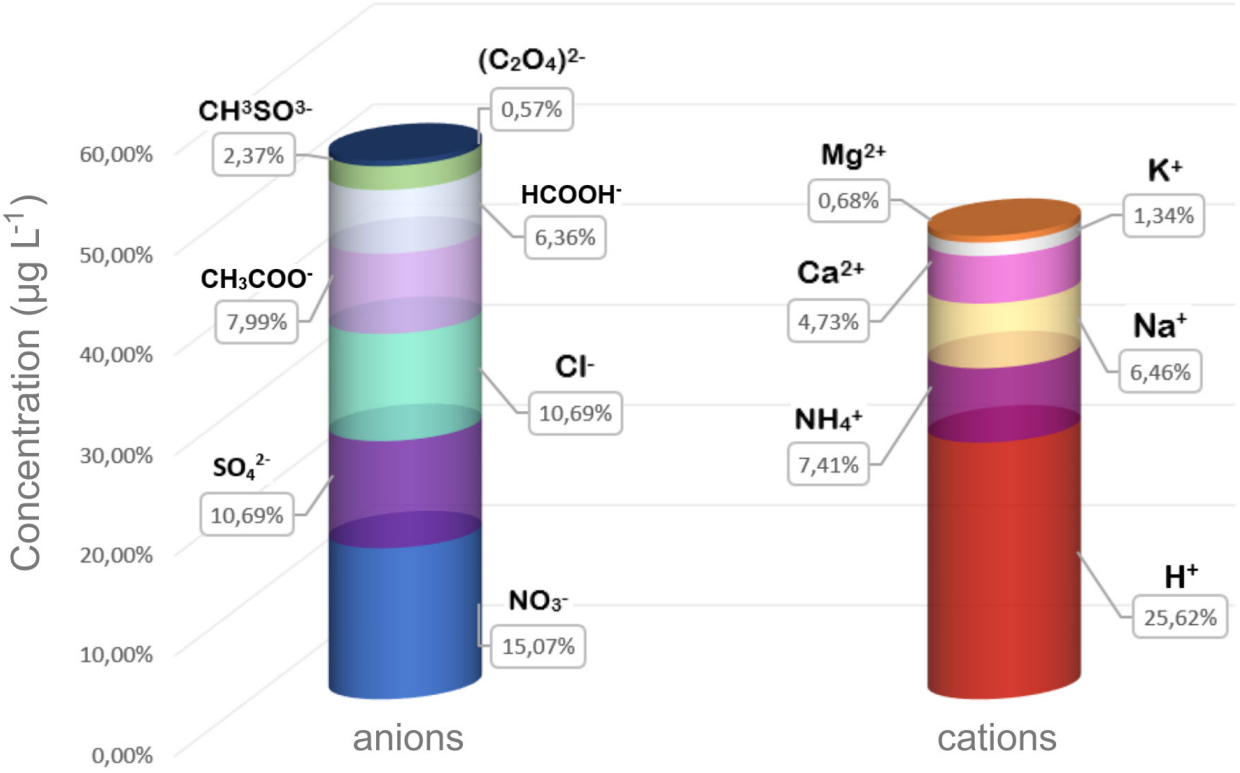

Figure 11. Average contribution, in percentage, of each analyte to the total ionic composition of TT-6. The values are arranged in decreasing order from the bottom to the top of each column, with anions represented in cold colors (left) and cations in warm colors (right). Source: authors.

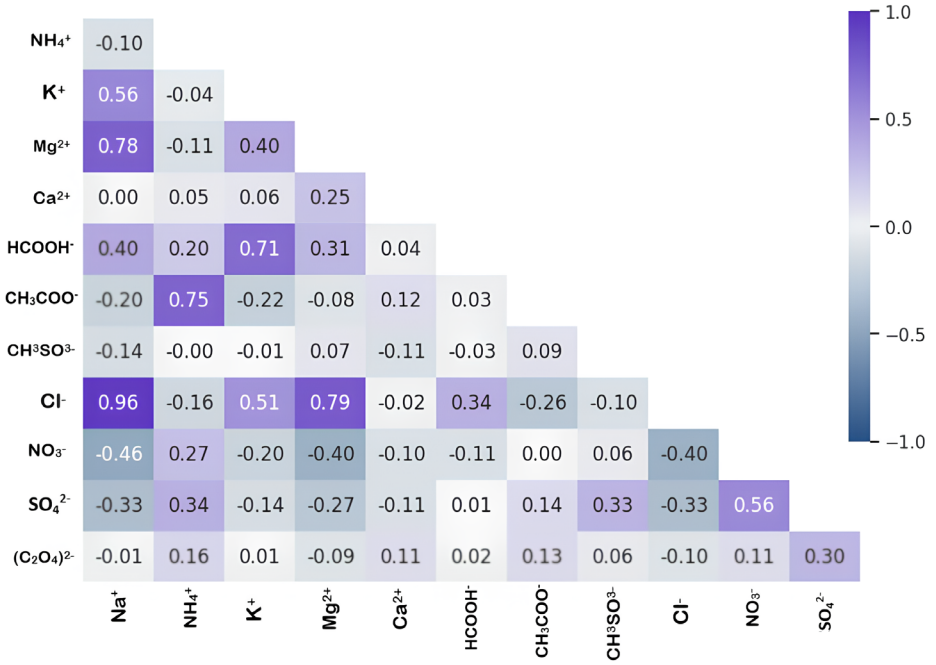

Figure 12. Correlation matrix calculated with r-Pearson. Purple tones indicate higher correlations, and gray tones indicate lower ones. This visualization assists in identifying related ions and estimating possible common source areas. For instance, Na^+ and Cl^-, predominantly from marine sources, have a correlation of 0.96. Source: authors.

Marine-derived aerosols: Sea salt contributions

The geographical position of the Antarctic continent renders it less susceptible to the arrival of continental aerosols resulting from anthropogenic pollution and mineral dust, making the sea spray the primary source of aerosols of marine origin (Dasarathy et al. 2023). Marine aerosols are primarily generated by wind agitation on the ocean surface, producing bubbles that burst and release a spray of particles into the atmosphere (Prather et al. 2013, Liu et al. 2021).

The analytes Na^+, Mg^+, K^+, Ca^{2+}, Cl^-, and SO_4^{2-} commonly appear in the composition of marine-origin aerosols (Legrand & Mayewski 1997, Thoen 2017). For sodium, calcium, and sulfate, there exist sets of equations distinguishing marine ("ss" for sea salt) from non-marine ("nss" for non-sea-salt) contributions to the total ion value.

To calculate nss sulfate, Equation 1 (Dixon et al. 2004), as mentioned in Section "Ions", "$nssSO_4^{2-} = SO_4^{2-} - (0.251\ x\ Na^+)$" was applied.

As for calcium and sodium, another study (Bigler et al. 2006) presents a system of equations to differentiate the marine and non-marine contributions of the Na^+ and Ca^+ (Equations 3 and 4, respectively). This system was calculated using values of 0.562 for $[Na^+/Ca^+]nss$ (Bigler et al. 2006) and 0.038 for $[Na^+/Ca^+]ss$ (Udisti et al. 2012).

Equation 3:

$$nss\,Ca^{2+} = c\{[Ca^{2+}] - [Na^+]*(\tfrac{Ca^{2+}}{Na^+})ss\}$$

$$where:\ c = [1 - (\tfrac{Na^+}{Ca^{2+}})nss*(\tfrac{Na^+}{Ca^{2+}})ss]^{-1}$$

Equation 4:

$$ss\,Na^+ = tot\,Na^+ - 0.562nss\,Ca^{2+}$$

The results of the calculations of marine and non-marine contributions to Na^+, Ca^+, and SO_4^{2-} are in Table VI.

The ions Ca^+ and SO_4^{2-} may also be part of marine salts; however, as the results for these analytes suggest a predominance of non-marine

Table VI. Separation of marine (ss) and non-marine (nss) contributions to Na^+ and Ca^+.

Ions	Total (tot)	Sea-salt (ss)	Non sea-salt (nss)
Na^+	16.29	96.38%	3.11%
Ca^+	11.9	3.62%	96.89%
SO_4^{2-}	26.37	15.50%	84.50%

sources, they will be addressed in individual topics.

Following Bigler's equations, Na^+ was found to have predominantly marine contributions, with 96.38% being ssNa^+. This result was expected, as sodium is commonly regarded as a reference marker for marine aerosols and constitutes the majority of coastal aerosols (Hall & Wolff 1998). At the onset of winter, before sea ice formation, intensified winds are responsible for increasing the load of aerosols transported to the continent's interior (Kaspari et al. 2005). This period is characterized by the formation of frost flowers. During freezing, water expels salt, forming brines on the surface. In this context, sulfate precipitates as mirabilite, $Na_2SO_4 10H_2O$ (Wolff et al. 2003), causing sulfate fractionation. At temperatures near -20°C, ice flowers can attain a salinity around three times higher than seawater (Rankin et al. 2002). Thus, Na^+ peaks are used to identify winter periods and can indicate changes in the intensity of zonal winds (Udisti et al. 2012).

For the TT-6 samples, the three highest correlations with Na^+ were found to be Cl^- (0.96), Mg^+ (0.78), and K^+ (0.56). Additionally, a significant correlation between Cl^- and Mg^{2+} indicates that they likely originate from the same source, namely marine salts. We can observe these behaviors in Figure 13.

It is noticeable that the highest peaks occurred in 2007, also identified as the warmest summer of the period in Figure 6, coinciding with the occurrence of an El Niño. The relationship between this type of climatic event and the increased transport of maritime air into the continent will be discussed in section "ENSO event impacts on snow core chemical signatures".

Crustal sources of calcium

Although calcium is also present in the ocean in forms such as calcium carbonate, its non-marine contribution appears as a soluble particle of mineral dust. It is interpreted as an indicator of a crustal source (Schüpbach et al. 2013). In TT-6, it was found that 96.89% of the calcium present is of non-marine origin, indicating a low correlation of this cation with others of marine origin. Observations over the extensive time series from the EPICA Domo C core (Lambert et al. 2011) indicate that calcium and insoluble dust follow cyclical climate patterns and show higher levels during cold periods.

The predominance of crustal contributions from calcium has also been observed in previous studies in West Antarctica (Lindau et al. 2016), which suggests the Ellsworth Mountains (Figure 1) as a possible source of this dust. According to Hoffman et al. (2020), the Weddell Sea sector is the main origin of air masses heading towards Union Glacier (79°46'00" S, 82°50'00" W), a direction of atmospheric transport that favors the arrival of particles at the TT-6 site.

Influence of non-sea-salt sulfate on the dating of glaciochemical records

Sulfate makes up an average of 26.37 μg L^{-1}, approximately 10% of the ionic content of TT-6. However, when applying the equation of Dixon

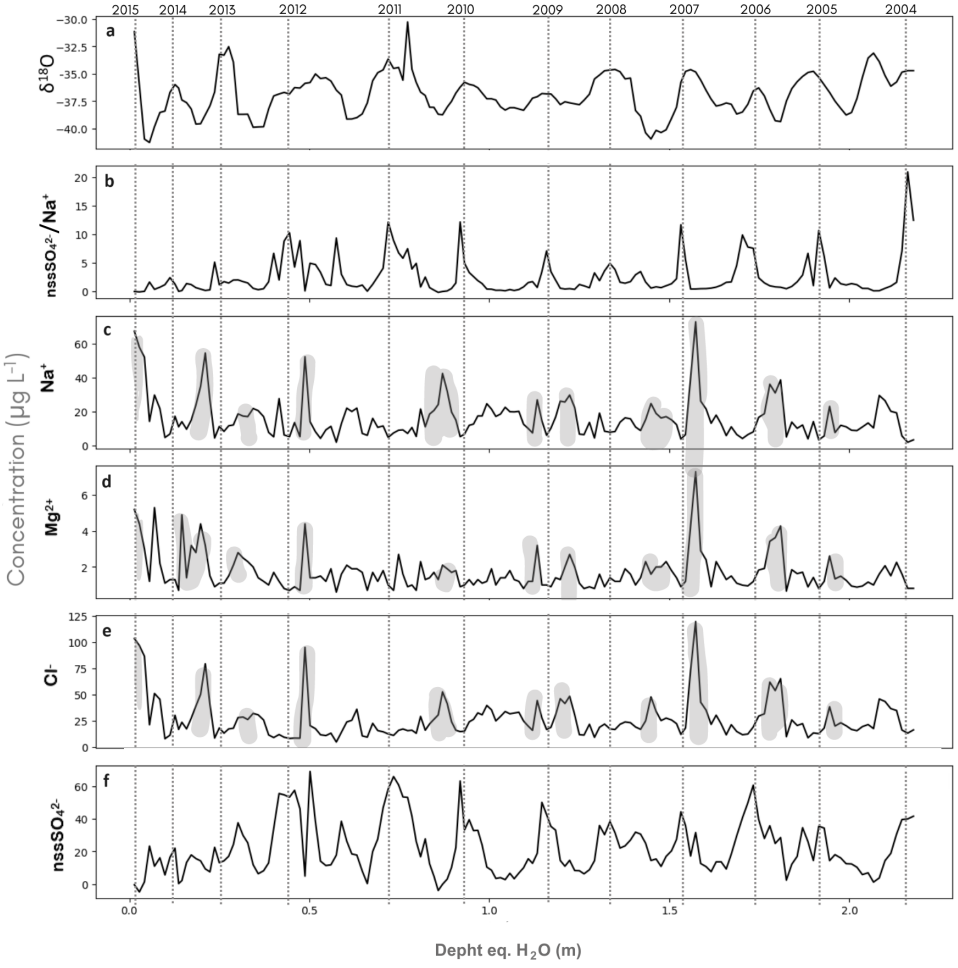

Figure 13. The TT-6 concentration profiles for Na^+, Mg^{2+}, K^+, and Cl^- demonstrate the high correlation between these analytes (indicating a common source, marine). Figures a, b, and f make up the table to illustrate the dating. The gray shading in figures c, d, and e indicates the peaks of marine ions. Source: authors.

(already demonstrated in section "Ions"), we note that 84.4% of this total corresponds to $nssSO_4^{2-}$. This aerosol originates from various sources, such as sea salt, volcanic gas, terrestrial dust, and anthropogenic activities (Uemura et al. 2022). When $nssSO_4^{2-}$ indicates volcanic sulfate contribution, it can be used to identify reference horizons that help validate the ice core dating.

Currently, in Antarctica, its main source is the metabolic activities of marine phytoplankton, which release this analyte into the environment through dimethylsulfide $(CH_3)_2S$ (Uemura et al. 2016). However, another study (Kunasek et al. 2010) analyzed the contribution of different sulfate isotopes in cores from the interior of Antarctica and found that the presence of volcanic or stratospheric sulfates is more significant in the WAIS region compared to the EAIS. This difference may be due to the lower elevation on the western side, contributing to aerosols' arrival by cyclones. Low $\delta^{34}S$ values were also found in the WAIS samples, indicating little sulfate from terrestrial continental sources in this region.

Nitrate variability: Seasonal and photochemical drivers

With an average concentration of 15.07%, nitrate is the most significant anion in the ionic composition of TT-6.

Looking at the r-Pearson matrix, we observe that nitrate has negative correlations with almost all the other analytes and is inversely

proportional to all the ions considered to come from sea salt, reaching -0.46 in correlation with sodium. This negative correlation can be explained by releasing nitrogen oxides (NO_2 and NO) that occur when snow is warmed by UV radiation and becomes photochemically active. Thus, sunlight oxidizes NO_2 to form nitric acid. Therefore, during the summer, with higher sunlight incidence, there is a greater concentration of nitric acid in the environment (Gonçalves et al. 2021), while marine salts have shown a higher presence in winter. Despite being further away, bird nesting sites also exhibit high rates of N_2 in the soil, which, when exposed to higher temperatures, denitrifies, releasing the compound into the environment (Neufeld et al. 2015).

There is also analytical interference due to the co-elution of nitrate and carbonate during the application of ion chromatography, a factor that may have underestimated the values obtained. However, this occurrence does not significantly compromise the NO_3^- data, as the average concentrations were within the expected range and far from the detection limits.

ENSO event impacts on snow core chemical signatures

Three large-scale climatic modes should be considered when observing variations in atmospheric transport in WAIS. The ENSO events (El Niño and La Niña) act by modifying the temperature of the Pacific Ocean waters. The Amundsen Sea Low (ASL) constitutes a low-pressure zone that moves seasonally between the Amundsen and Bellingshausen Seas, facilitating the entry of marine air into the continent, which can increase precipitation and temperature in some regions (Raphael et al. 2016). The Southern Annular Mode (SAM) circulates extratropical air masses in the Southern Hemisphere (Caldas et al. 2020). It is described as a seesaw (Thompson & Wallace 2000) because it modulates the influence of tropical masses on polar masses, balancing the pressure gradients between them.

The influence of El Niño can favor and sustain the entry of warmer marine air into the continent. When this event occurs in conjunction with a negative SAM phase, meridional heat exchange is facilitated, increasing the likelihood of warm events (Nicolas et al. 2017). According to the Oceanic Niño Index on the National Oceanic and Atmospheric Administration (NOOA) website (NOAA 2024), during the years that make up TT-6, there were four El Niño and five La Niña (Table VII).

The ERA5 results contributed to our understanding of the physical behavior of snow deposited at the TT-6 site, providing values for the accumulation rate, albedo, and temperature, and they also corroborated the observations related to the core's chemical composition and its constituent ions. When considering ENSO events and ion concentrations, we observed that some of the highest peaks in marine aerosols (Na^+, Mg^{2+}, and Cl^-), as shown in Figure 14, coincide with El Niño events, suggesting a potential influence of these events on ion concentrations. The most prominent peaks were recorded during the 2006/2007 El Niño, a period also marked by the warmest summer (Figure 7) of the study, with average wind speeds reaching 72 km/h, likely facilitating the transport of these aerosols inland.

Following this event, ion concentrations decreased but rose again at the end of 2011, a year with the warmest winter in the analyzed period, despite being a La Niña year. Additionally, wind data reanalysis showed the highest average wind speed in the study period, reaching 75 km/h, indicating that other climatic factors also contribute to the concentration of marine ions in the continent's interior.

Table VII. El Niño and La Niña Events within the period represented by TT-6 snow samples.

Data	Jan	Feb	Mar	Apr	May	Jun	Jul	Aug	Sep	Oct	Nov	Dec
2004							El Niño	El Niño	El Niño	El Niño	El Niño	El Niño
2005	El Niño	El Niño									La Niña	La Niña
2006	La Niña	La Niña	La Niña						El Niño	El Niño	El Niño	El Niño
2007	El Niño					La Niña	La Niña	La Niña	La Niña	La Niña	La Niña	La Niña
2008	La Niña	La Niña	La Niña	La Niña	La Niña	La Niña					La Niña	La Niña
2009	La Niña	La Niña	La Niña				El Niño	El Niño	El Niño	El Niño	El Niño	El Niño
2010	El Niño	El Niño	El Niño			La Niña	La Niña	La Niña	La Niña	La Niña	La Niña	La Niña
2011	La Niña	La Niña	La Niña	La Niña	La Niña		La Niña	La Niña	La Niña	La Niña	La Niña	La Niña
2012	La Niña	La Niña	La Niña	La Niña								
2013												
2014										El Niño	El Niño	El Niño
2015	El Niño											

CONCLUSIONS

The analyses conducted in this study allowed for the reconstruction of the climate variability at the TT-6 core site for 11 years ± 6 months when the mean annual snow accumulation rate was 0.19 ± 0.02 m in water equivalent. The ionic concentrations obtained are similar to those in previous studies in this site's region (Schwanck 2016, Thoen et al. 2018).

The time series constructed with the ions Na^+ and SO_4^{2-} and their ratio showed coherent seasonality, with peaks at times inverse to those in oxygen isotopes. The isotopic results have a correlation of 0.99 with the Antarctic Meteoric Line. The identification of the Puyehue eruption, with the peak of $nssSO_4$ in 2011, also contributed to the increase in the precision of the core dating.

The ionic balance indicates that TT-6 comprises a more significant contribution of anions (53.73%). When grouping the ions based on Pearson's correlations, there was no discrepancy with the natural distribution of these chemical species, highlighting the effectiveness of using statistics in this data analysis. We estimate that 96.86% of the calcium and 84.50% of the sulfate are of non-sea origin. Bigler's calculation shows that 96.38% of Na^+ is of marine origin. Therefore, Cl^- and Mg^{2+}, which correlate greater than 75% with sodium and similar seasonal behavior (peaks in winter), were also considered marine.

In climate data from the ERA5 model, an albedo of 0.8 (on a scale of 0 to 1) was identified

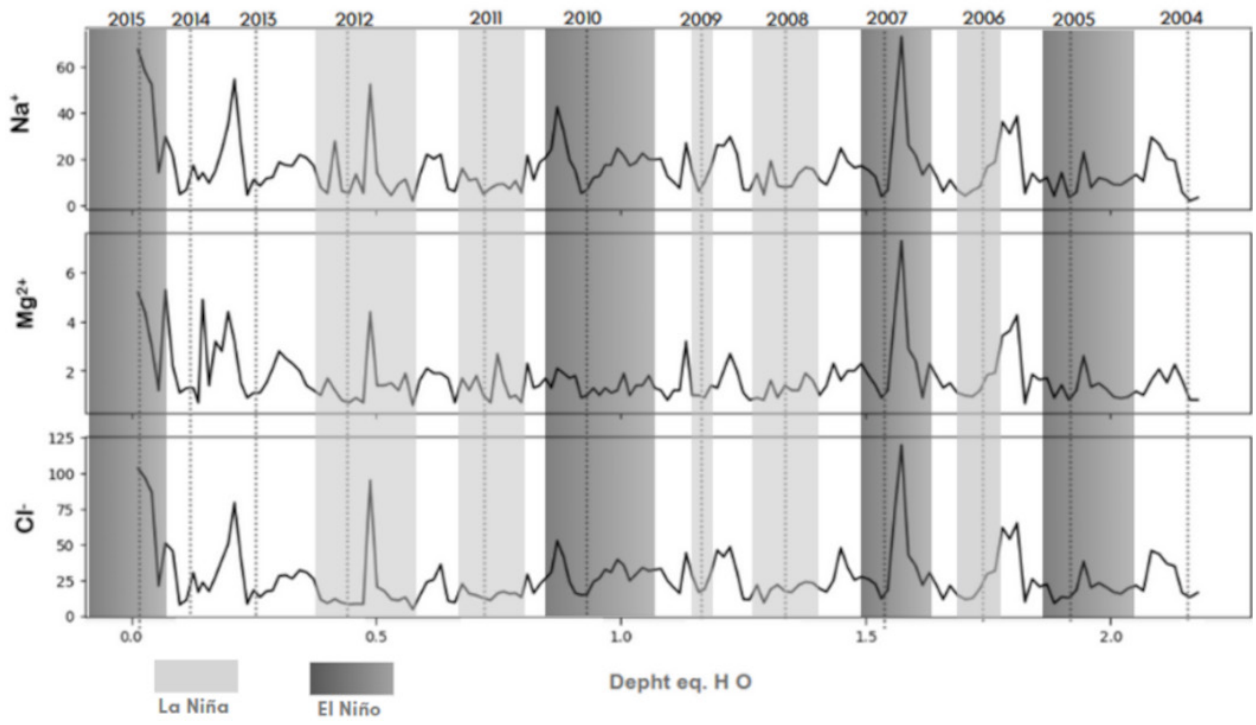

Figure 14. Time series of ions predominantly of marine origin (Na^+, Mg^{2+}, and Cl^-) along with El Niño and La Niña events from 2004 to 2015. Light gray vertical bands indicate La Niña periods, while dark gray bands represent El Niño periods. The highest peaks in the series coincide with the 2006 El Niño event. Source: authors.

at the TT-6 site, and the predominance of south and southwest winds, between 180° and 225°, with an average speed of 18 km h^{-1}. The ERA5 temperature reanalysis shows that the hottest summer of the period occurred in 2007, marking -18.6°C, in the same year that the most prominent peaks of marine aerosols occurred. This relationship may be due to the influence of El Niño that year, which facilitates the atmospheric transport from the ocean to the continent. The maximum wind speed reinforced this assumption in 2007, 72 km h^{-1}, the second highest recorded in the period.

Acknowledgments

This research is part of the Programa Antártico Brasileiro (PROANTAR) and was financed by the Conselho Nacional de Desenvolvimento Científico e Tecnológico (CNPq), process 557053/2009-9, and from the Instituto Nacional de Ciência e Tecnologia da Criosfera (CNPq process 465680/2014-3). We thank our colleagues Filipe G.L. Lindau and Luciano Marquetto for their support during the fieldwork.

REFERENCES

ANZANO J, ABÁS E, MARINA-MONTES C, VALLE JD, GALÁN-MADRUGA D, LAGUNA M, CABREDO S, PÉREZ-ARRIBAS L, CÁCERES J & ANWAR J. 2022. A Review of Atmospheric Aerosols in Antarctica: from characterization to data processing. Atmosphere 13: 1621.

BIGLER M, RÖTHLISBERGER R, LAMBERT F, STOCKER TF & WAGENBACH D. 2006. Aerosol deposited in East Antarctica over the last glacial cycle: detailed apportionment of continental and sea salt contributions. J Geophys Res 111: 1-14.

CALDAS CF, VASCONCELLOS FC, CAVALCANTI IFA, CARVALHO NO & LOPES IR. 2020. Impacto do Gelo Marinho Antártico, do ENOS e do Modo Anular Sul sobre as Frentes Frias na América do Sul. Anu Inst de Geocienc 43: 229-237.

CRAIG H. 1961. Isotopic variations in meteoric waters. Science 133(3465): 1702-1703.

DASARATHY S, RUSSELL LM, RODIER SD & BOWMAN JS. 2023. Wind-driven and seasonal effects on marine aerosol

production in the Bellingshausen Sea, Antarctica. Geophys Res Lett 50: 1-10.

DIXON D, MAYEWSKI PA, KASPARI S, SNEED S & HANDLEY M. 2004. A 200 year sub-annual record of sulfate in West Antarctica, from 16 ice. Ann Glaciol 39: 545-556.

FERREIRA R. 2024. Raw data of Antarctic snow core BRTT6 UFRGS [Data set]. Zenodo Repository.

GONÇALVES SJ, WEIS J, CHINA S, EVANGELISTA H, HARDER TH, MÜLLER S, SAMPAIO M, LASKIN A, GILLES MK & GODOI RHM. 2021. Photochemical reactions on aerosols at West Antarctica: a molecular case-study of nitrate formation among sea salt aerosols. Sci Total Environ 758: 1-8.

HALL JS & WOLFF EW. 1998. Causes of seasonal and daily variations in aerosol sea-salt concentrations at a coastal Antarctic station. Atmos Environ 32: 3669-3677.

HERSBACH H ET AL. 2023. ERA5 monthly averaged data on single levels from 1940 to present. Copernicus Climate Change Service (C3S).

HERSBACH H ET AL. 2020. The ERA5 global reanalysis. Q J R Meteorol Soc 146: 1999-2049.

HOFFMANN K ET AL. 2020. Stable water isotopes and accumulation rates in the Union Glacier region, Ellsworth Mountains, West Antarctica, over the last 35 years. Cryosphere 14: 881-904.

JAKOBSSON M, ANDERSON JB, NITSCHE FO, GYLLENCREUTZ R, KIRSHNER AE, KIRCHNER N, O'REGAN M, MOHAMMAD R & ERIKSSON B. 2012. Ice sheet retreat dynamics inferred from glacial morphology of the central Pine Island Bay Trough, West Antarctica. Quat Sci Rev 38: 1-10

JOUZEL J. 2013. Water Stables Isotopes: Atmospheric Composition and Applications in Polar Ice core Studies. 2nd ed., Treatise on Geochemistry, vol. 5, Elsevier Ltd.

KASPARI S, DIXON DA, SNEED SB & HANDLEY M J. 2005. Sources and transport pathways of marine aerosol species into West Antarctica. Ann Glaciol 41: 1-9.

KUNASEK SA, ALEXANDER B, STEIG EJ, SOFEN ED, JACKSON TL, THIEMENS MH, MCCONNELL JR, GLEASON DJ & AMOS HM. 2010. Sulfate sources and oxidation chemistry over the past 230 years from sulfur and oxygen isotopes of sulfate in a West Antarctic ice core. J Geophys Res 115: 1-13.

LAMBERT F, BIGLER M, STEFFENSEN JP, HUTTERLI M & FISCHER H. 2011. The calcium-dust relationship in high-resolution data from Dome C, Antarctica. Clim Past Discuss 7: 1113-1137.

LEGRAND M & MAYEWSKI P. 1997. Glaciochemistry of polar ice cores: a review. Rev Geophys 35: 219-243.

LINDAU FGL, SIMÕES JC, MARQUES MM, HAMMER DF, SILVA DB, CASASSA G, SNEED S & INTRONE D. 2016. Variabilidade do conteúdo iônico da neve e do firn ao longo de um transecto antártico. Pesq Geociências 43: 213-228.

LINDOW J, CASTEX M, WITTMANN H, JOHNSON JS, LISKER F, GOHL K & SPIEGEL C. 2014. Glacial retreat in the Amundsen Sea sector, West Antarctica – first cosmogenic evidence from central Pine Island Bay and the Kohler Range. Quat Sci Rev 98: 66-173.

LIU S, LIU C, FROYD KD, SCHILL GP, MURPHY DM, BUI TP, DEAN-DAY JM, WEINZIERL B, DOLLNER M & DISKIN GS. 2021. Sea spray aerosol concentration modulated by sea surface temperature. PNAS 118: 1-6.

MARCHER A, BERNARDO RT, SIMÕES JC & AUGER J. 2022. Water stable isotopes in snow along a traverse of the West Antarctic Ice Sheet: insights into moisture origins, air-masses distillation history, and climatic value. An Acad Bras Cienc 94: e20210353. DOI 10.1590/0001-3765202220210353.

MASSON-DELMOTTE V ET AL. 2008. A Review of Antarctic Surface Snow Isotopic Composition: Observations, Atmospheric Circulation, and Isotopic Modeling. J Clim 21: 3359-3387.

NEUFELD ADH, GODOI SG, PEREIRA AB, BAYER C, SCHÜNEMANN AL, VICTORIA FDC, ALBUQUERQUE MP, CAMARGO E & VIEIRA FCB. 2015. Methane and nitrous oxide fluxes in relation to vegetation covers and bird activity in ice-free soils of Rip Point, Nelson Island, Antarctica. Polar Res 34: 1-12.

NICOLAS JP & BROMWICH DH. 2011. Climate of West Antarctica and Influence of Marine Air Intrusions. J Clim 24: 49-67.

NICOLAS JP ET AL. 2017. January 2016 extensive summer melt in West Antarctica favoured by strong El Niño. Nat Commun 8: 1-10.

NOAA. 2024. "El Niño-Southern Oscillation (ENSO) Index." Available at: https://origin.cpc.ncep.noaa.gov/products/analysis_monitoring/ensostuff/ONI_v5.php.

OSTERBERG EC, HANDLEY MJ, SNEED SB, MAYEWSKI PA & KREUTZ KJ. 2006. Continuous ice core melter system with discrete sampling for major ion, trace element, and stable isotope analyses. Environ Sci & Technology 40: 3355-3361.

PRATHER KA, BERTRAM TH, GRASSIAN VH, DEANE GB, STOKES MD, DEMOTT PJ, ALUWIHARE LI, PALENIK BP, AZAM F & SEINFELD JH. 2013. Bringing the ocean into the laboratory to probe the chemical complexity of sea spray aerosol. PNAS 110: 7550-7555.

RANKIN AM, WOLFF EW & MARTIN S. 2002. Frost flowers: implications for tropospheric chemistry and ice core interpretation. J Geophys Res 107: 1-17.

RAPHAEL MN, MARSHALL GJ, TURNER J, FOGT RL, SCHNEIDER D, DIXON DA, HOSKING JS, JONE JM& HOBBS WR. 2016. The Amundsen Sea Low: variability, change, and impact on Antarctic climate. Bull Am Meteorol Soc 97: 111-121.

SCHIPPER CI, CASTRO JM, TUFFEN H, JAMES MR & HOW P. 2013. Shallow vent architecture during hybrid explosive–effusive activity at Cordón Caulle (Chile, 2011–12): evidence from direct observations and pyroclast textures. J Volcanol 262: 25-37.

SCHÜPBACH S, FEDERER U, KAUFMANN PR, ALBANI S, BARBANTE C, STOCKER TF & FISCHER H. 2013. High-resolution mineral dust and sea ice proxy records from the Talos Dome ice core. Clim Past 9: 2789-2807.

SCHWANCK FC. 2016. Variabilidade química e climática no registro do testemunho de gelo Mount Johns – Antártica. Tese de doutorado, Universidade Federal do Rio Grande do Sul, 146 p.

THOEN IU. 2017. Conteúdo Iônico em testemunhos de firn/gelo do Monte Johns. Antártica Ocidental: 1882-2008. Tese de mestrado, Universidade Federal do Rio Grande do Sul, 133 p. (Unpublished).

THOEN IU, SIMÕES JC, LINDAU FGL & SNEED SB. 2018. Ionic content in an ice core from the West Antarctic Ice Sheet: 1882-2008 A.D. Braz J Geol 48: 853-865.

THOMPSON DWJ & WALLACE JM. 2000. Annular Modes in the Extratropical Circulation. Part I: Month-to-Month Variability. J Climate 13: 1000-1016.

TURNER J & PENDLEBURY S. 2004. The International Antarctic Weather Forecasting Handbook. Cambridge: British Antarctic Survey, 663 p.

UEMURA R, MASAKA K, FUKUI K, IIZUKA Y, HIRABAYASHI M & MOTOYAMA H. 2016. Sulfur isotopic composition of surface snow along a latitudinal transect in East Antarctica. Geophys Res Lett 43: 5878-5885.

UEMURA R, MASAKA K, IIZUKA Y, HIRABAYASHI M, MATSUI H, MATSUMOTO R, UEMURA M, FUJITA K & MOTOYAMA H. 2022. Soluble salts in deserts as a source of sulfate aerosols in an Antarctic ice core during the last glacial period. Earth Planet Sci Lett 578: 1-10.

UDISTI R, DAYAN U, BECAGLI S, BUSETTO M, FROSINI D, LEGRAND M, LUCARELLI F, PREUNKERT S, SEVERI M & TRAVERSI R. 2012. Sea spray aerosol in central Antarctica. Present atmospheric behaviour and implications for paleoclimatic reconstructions. Atmos Environ 52: 109-120.

WOLFF EW, RANKIN AM & RÖTHLISBERGER R. 2003. An ice core indicator of Antarctic sea ice production? Geophys Res Lett 30: 1-4.

How to cite

FERREIRA RS, SIMÕES JC, THOEN IU & BERNARDO RT. 2024. Glaciochemistry and environmental interpretation of a snow core from West Antarctica. An Acad Bras Cienc 96: e20240243. DOI 10.1590/0001-3765202420240243.

Manuscript received on March 9, 2024;
accepted for publication on November 7, 2024

REGINA S. FERREIRA[1]
https://orcid.org/0000-0001-9918-6340

JEFFERSON C. SIMÕES[1,2]
https://orcid.org/0000-0001-5555-3401

ISAÍAS U. THOEN[1]
https://orcid.org/0000-0002-2419-8838

RONALDO T. BERNARDO[1]
https://orcid.org/0000-0002-1143-7916

[1]Universidade Federal do Rio Grande do Sul,
Centro Polar e Climático, Av. Bento Gonçalves,
9500, 91501-970 Porto Alegre, RS, Brazil

[2]Climate Change Institute, University of Maine, Sawyer
Research Building, 133, Orono, ME 04469, EUA

Correspondence to: **Regina Souza Ferreira**
E-mail: regina.souzaf@hotmail.com

Author contributions

Regina S. Ferreira wrote this manuscript and processed and interpreted the analyses. Isaias U. Thoen and Ronaldo T. Bernardo conducted fieldwork, decontaminated the snow core, subsampled it, and supervised laboratory analyses. Jefferson C. Simões coordinated the project, participated in the fieldwork, reviewed the article, and contributed to discussions.